Chapter 2: The nature of tidal signals

2.1 Introduction

Much of this study is concerned with the identification and analysis of tidal signals in hydrothermal systems associated with mid-ocean ridge. Consequently, it is appropriate to define the term tidal signal before proceeding any further. An observer at rest on the Earth experiences a force per unit mass due to the gravitational attraction of celestial bodies. This is known as the tide-generating force and is the spatial gradient of a function known as the tidal potential (W) (Melchior, 1983).

A tidal signal can then be defined to be any time-series, or component of a time-series, whose cause is the tidal potential. Generally, time-series are influenced by many physical processes, some of which are independent of the tidal potential. It is often helpful to decompose an empirical time-series into two parts: a tidal signal; and a residual signal containing the contributions of noise, instrumental drift and other physical processes. (In Chapter 3, an explicit formalism for splitting the residual into a drift signal and a noise signal is discussed.)

There are many observable consequences of the tidal potential - of which the rise and fall of the oceans (the ocean tide) and associated horizontal currents (tidal streams) are the most commonly known. Less obviously, the Earth's crust is deformed directly by the tide-generating force (to produce the solid tide) and by the weight of the shifting oceans (to produce the load tide). All of these phenomena produce tidal signals. In every case there is a well-understood physical mechanism by which the tidal potential causes the observable time-series. In addition, each of these signals has a frequency spectrum which is similar to that of the tidal potential, in the sense that it contains power at the same discrete set of frequencies and in roughly the same proportions. It must be stressed that tidal signals are not required, by definition, to have these typically tidal spectra. Nonetheless, it appears that many of them do. This is because their dependence on the tidal potential is approximately linear.

In particular, it is often the case that the physical process linking the local tidal potential ($W(t)$) to an observable time-series ($\zeta(t)$) can be well approximated by a time-domain convolution with a response function $r(t)$ (Munk & Cartwright, 1966):

$$\zeta(t) = \int_{\tau=-\infty}^{\infty} r(\tau) \cdot W(t-\tau) d\tau \tag{2.1}$$

By taking Fourier transforms:

$$\hat{\zeta}(f) = \int_{t=-\infty}^{\infty} \zeta(t) \cdot e^{2\pi i f t} dt, \quad R(f) = \int_{t=-\infty}^{\infty} r(t) \cdot e^{2\pi i f t} dt, \quad \hat{W}(f) = \int_{t=-\infty}^{\infty} W(t) \cdot e^{2\pi i f t} dt \tag{2.2}$$

the convolution can be transformed into a multiplication in the frequency domain:

$$\hat{\zeta}(f) = R(f) \cdot \hat{W}(f) \tag{2.3}$$

Hence, provided that the admittance ($R(f)$) is a reasonably smooth function of frequency (f) the process $\zeta(t)$ will have a similar spectrum to the tidal potential $W(t)$.

Regardless of whether a time-series ($\zeta(t)$) really does depend on the tidal potential in this linear fashion it is of interest to examine its frequency spectrum. A spectrum containing power at the typical tidal frequencies may be taken as strong evidence that the signal under analysis is influenced by the tidal potential.

The tidal potential has a highly distinctive power spectrum, which can be calculated to great precision. It is reasonable to expect that any tidal signal will exhibit similar behaviour. For this reason, it is of great benefit to review the nature of the tidal potential in considerable detail, before considering any data which might be affected by it.

The next step is to identify, *a priori*, some plausible physical mechanisms by which the tidal potential might affect seafloor hydrothermal systems. The first order effects of the tidal potential (the solid, ocean and load tides, as well as tidal streams) are examined in turn. Qualitative estimates are then made of how these first order effects might lead to the second order effects (variations in temperature, flow rate and effluent chemistry) observed at hydrothermal systems.

2.2 The Tidal Potential of a celestial body

By definition, all tidal phenomena on Earth are caused by the gravitational fields of celestial bodies. Every astronomical object creates tidal forces on Earth, but it is the contributions from the moon and the sun which are, by far, the most important (Doodson & Warburg, 1941). Consequently, it is only the lunar and solar tides which are considered here.

At any fixed point on the Earth's surface, the tidal potential changes over time as the moon and the sun move with respect to the rotating Earth. Two spherical co-ordinate systems are commonly used to describe this motion – the ecliptic system and the equatorial system. Their relationship is summarised in Figure 2.1.

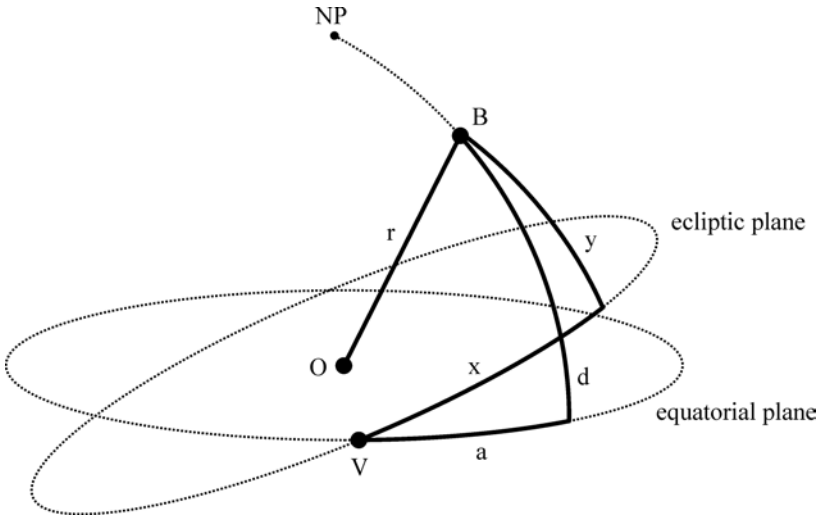

Figure 2.1: The position of a tide-raising body, *B*, relative to the centre of the Earth, *O*, and the vernal equinox, *V*. The point *NP* is the celestial North Pole. In equatorial coordinates, the point *B* is described by the triple (*r,a,d*). In ecliptic coordinates, it is described by the triple (*r,x,y*). Coordinates are named as follows: *r* - distance from the centre of the Earth, *a* - right ascension, *d* – declination, *x* – ecliptic longitude, *y* – ecliptic latitude. Figure adapted from Doodson & Warburg (1941).

Consider the tidal potential at a point *P* due to a single tide-raising body *B* of mass M_B (Figure 2.2). The tide-raising body lies at a distance r_B from the centre of the earth, and at a declination *d* above the equator.

The tidal potential at *P*, W(r,λ,Z), can be written as a sum of spherical harmonic functions. For practical purposes, $W(r,\lambda,Z)$ is approximated to sufficient accuracy by the first term in this series, the second order spherical harmonic function $W_2(r,\lambda,Z)$ (Melchior, 1983; Doodson & Warburg, 1941).

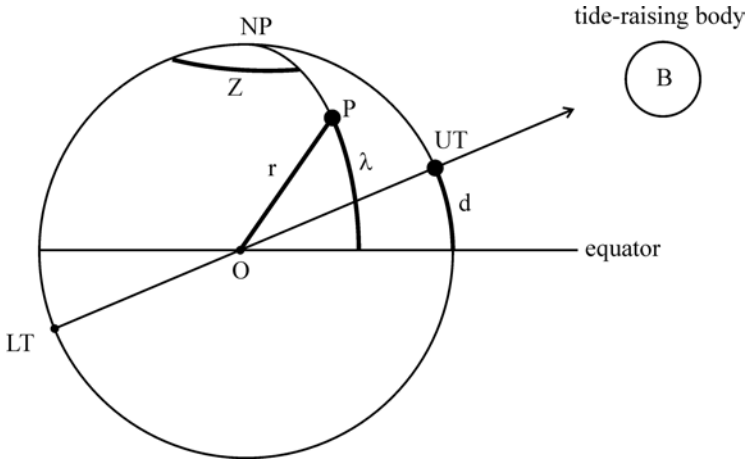

Figure 2.2: The tidal potential W at a point P on the Earth's surface, due to a single tide-raising body B with declination d. NP is the North Pole. UT is the point of upper transit, directly below the tide-raising body. The location of P can described by (r,λ,Z), where r is distance to the centre of the Earth, λ is (terrestrial) latitude and Z is the angle between the meridian of lower transit (LT) and the meridian of the point P. The tidal potential at P is $W(r,\lambda,Z)$ as described in the text. Figure adapted from Doodson &Warburg (1941).

If G is the gravitational constant, $W_2(r,\lambda,Z)$ is defined by:

$$W_2(r,\lambda,Z) = \frac{3}{4}\left[GM_B\frac{r^2}{r_B^3}\right]\begin{Bmatrix}\cos^2(\lambda)\cos^2(d)\cos(2Z)\ldots\\ \ldots-\sin(2\lambda)\sin(2d)\cos(Z)\ldots\\ \ldots+3\left(\sin^2(\lambda)-\frac{1}{3}\right)\cdot\left(\sin^2(d)-\frac{1}{3}\right)\end{Bmatrix} \quad (2.4)$$

It is very important that the tidal potential due to a tide-raising body varies over two separate timescales. Firstly, there is a short timescale associated with the rotation of the Earth. The angle ($Z(t)$) between the meridian of the tide-raising body and the meridian of the point P increases at a rate of ~15º per hour (or ~360º per day). Consequently, the tidal potential at P displays diurnal ($\cos(Z)$) and semi-diurnal ($\cos(2Z)$) periodicity. Secondly, there is a long timescale, associated with the oscillations in declination $d(t)$ and distance $r_B(t)$ of the tide-raising body. These oscillations have a period of ~1 month when the tide-raising body is the moon, and ~1 year when it is the sun. The interaction of periodic processes on these short (daily) and long (monthly and yearly) timescales leads to the characteristic spectral nature of tidal phenomena (Section 2.3.4).

Time-series measurements of hydrothermal systems often span a time interval intermediate between these short and long timescales (Chapter 4). In Chapter 3, it is shown that this has important implications for the extraction of tidal information from a seafloor dataset.

2.3 Decomposition of the Tidal Potential

2.3.1 Decomposition by species

Defining M_E to be the mass of the Earth, and r_E to be the radius of the Earth, the gravitational acceleration at the Earth's surface (g) is given by:

$$g = \frac{GM_E}{r_E^2} \tag{2.5}$$

Hence, the tidal potential at the Earth's surface, due to a single tide-raising body, is:

$$W_2\big|_{r=r_E} = gr_E \frac{3}{4}\left[\frac{M_B}{M_E}\left(\frac{r_E}{r_B}\right)^3\right]\begin{cases}\cos^2(\lambda)\cos^2(d)\cos(2Z)\ldots \\ \ldots - \sin(2\lambda)\sin(2d)\cos(Z)\ldots \\ \ldots + 3\left(\sin^2(\lambda)-\frac{1}{3}\right)\cdot\left(\sin^2(d)-\frac{1}{3}\right)\end{cases} \tag{2.6}$$

This can be split into three species by considering the three terms on the right hand side of equation (2.6).

The first species, known as the long-period species, consists of the term:

$$gr_E \frac{3}{4}\left[\frac{M_B}{M_E}\left(\frac{r_E}{r_B}\right)^3\right]3\left(\sin^2(\lambda)-\frac{1}{3}\right)\cdot\left(\sin^2(d)-\frac{1}{3}\right) \tag{2.7}$$

This expression changes over time because of the long timescale changes in the distance $r_B(t)$ and declination $d(t)$ of the tide-raising body. The exact formulae for $r_B(t)$ and $d(t)$ need not be quoted here. It is sufficient to note that they have been calculated to great precision for both the moon and the sun (Doodson & Warburg, 1941), and are available in public domain computer codes such as ETGTAB and CSR. (Further details of these and other computer codes used in this dissertation are given at the end of the References section.)

There are two short timescale species, known as the diurnal and semi-diurnal species. The diurnal species of the tidal potential consists of the term:

$$-gr_E \frac{3}{4}\left[\frac{M_B}{M_E}\left(\frac{r_E}{r_B}\right)^3\right]\sin(2\lambda)\sin(2d)\cos(Z) \tag{2.8}$$

Here, the presence of the earth rotation term cos(Z) means that a short timescale diurnal oscillation interacts with the long timescale changes in $r_B(t)$ and $d(t)$. It is helpful to think of the diurnal species as being a diurnal oscillation (cos(Z)) whose amplitude is modulated over the long timescale by the declinational term sin(2d). (The changes in distance ($r_B(t)$) have a similar but less significant effect.) It follows that the diurnal part of the tidal potential is greatest when the declination of the tide-raising body is greatest (Section 2.3.2).

Finally, the semi-diurnal species of the tidal potential consists of the term:

$$gr_E \frac{3}{4}\left[\frac{M_B}{M_E}\left(\frac{r_E}{r_B}\right)^3\right]\cos^2(\lambda)\cos^2(d)\cos(2Z) \tag{2.9}$$

The semi-diurnal species can be considered to be a semi-diurnal oscillation (cos(2Z)), whose amplitude is modulated over the long timescale by the declinational term cos^2(d). Therefore, the semi-diurnal part of the tidal potential is greatest when the declination of the tide-raising body is zero (Section 2.3.2).

2.3.2 Frequency Modulation by declinational changes

The decomposition of the tidal potential into species (Section 2.3.1) is conceptually useful when considering tidal phenomena over a timescale of a few days. On such a timescale, changes in the distance and declination of a tide-raising body can give the tidal potential a non-stationary appearance (Figure 2.3).

In the example shown in Figure 2.4, the lunar declination (d) is zero approximately 11 days into the time interval (Figure 2.3). At this time, the semi-diurnal species (with its cos^2(d) term) dominates over the diurnal species (with its sin(2d) term) in the tidal potential. Consequently, the tidal potential appears to be strongly semi-diurnal when viewed over the course of a few cycles at the centre of the observation period. However, at the beginning and end of the time interval, the lunar declination is large and the tidal potential has a dominantly diurnal appearance. The tidal potential as a whole can therefore be considered to be frequency-modulated by declinational changes. (In this example, attention has been focussed solely on the lunar declination because it varies appreciably over the course of 20 days. In principle, changes in solar declination have a similar effect. However, the period of change of solar declination is one year, and so the solar declination is therefore approximately constant.)

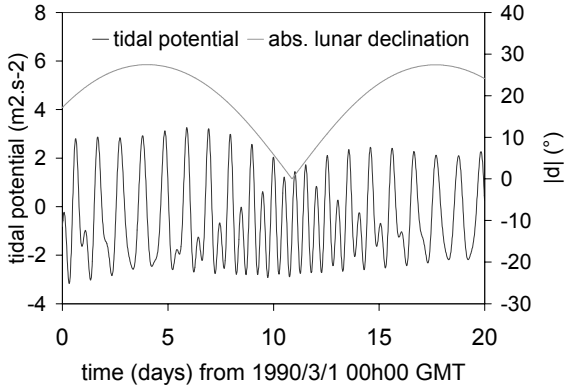

Figure 2.3: 'Frequency Modulation' of the tidal potential due to changes in lunar declination (d). The absolute value of the lunar declination ($|d|$) is plotted over a period of 20 days in March 1990. Also shown is the tidal potential, W, at (45°N, 0°E) over the same time interval. When the lunar declination is zero, the tidal potential is dominated by the semi-diurnal species. Conversely, the diurnal species dominates when the lunar declination is large. Data calculated using ETGTAB.

This phenomenon has important consequences for the interpretation of tidal data from hydrothermal systems. For example, if an observed seafloor time-series spans no more than a few days, it would be unwise to conclude that a frequency spectrum obtained from the dataset were typical. A dataset collected the following week might have a markedly different spectrum simply because of changes in lunar declination.

It is reasonable to suppose that any tidal signal will display some degree of diurnal/semi-diurnal frequency modulation, and it is of interest to see how such modulation correlates with the well-known astronomical forcing. For example, an observed tidal signal might display its greatest semi-diurnal character a few days *after* the lunar declination is zero. This would be evidence for a considerable time lag in the physical mechanism by which the tidal potential gave rise to the tidal signal.

2.3.3 Amplitude Modulation by lunar phase – spring and neap tides

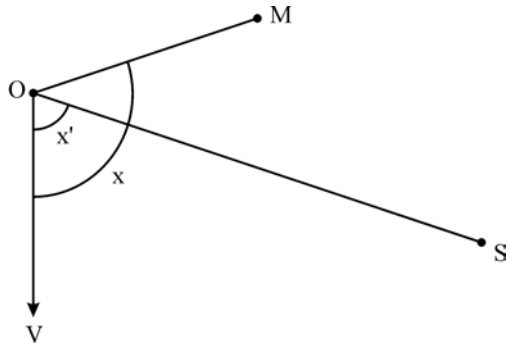

Figure 2.4: The positions of the sun (*S*) and moon (*M*) projected onto the ecliptic plane. The point *O* is the centre of the Earth. The moon and sun have ecliptic longitudes *x* and *x'* respectively, measured positive eastwards from the vernal equinox, *V*. A lunar phase parameter (Φ_L) can be defined by $\Phi_L=|\cos(x-x')|$.

For simplicity, the tidal potential due to a *single* tide-raising body is considered above (Section 2.3.1). However, the interaction of the lunar and solar tides creates an important phenomenon - the amplitude modulation of the tidal potential according to the phases of the moon (Doodson & Warburg, 1941).

When the moon is new or full, the lunar and solar potentials are in phase and produce spring tides which exhibit a larger range than normal. At half-moon, the tidal potentials are out of phase and produce neap tides, with a smaller range than normal. For this reason it is useful to define a lunar phase parameter (Φ_L) as a numerical measure of the phase of the moon.
If *x* is the ecliptic longitude of the moon, and *x'* is the ecliptic longitude of the sun (Figure 2.4), then Φ_L can be defined as follows:

$$\Phi_L = \left|\cos(x - x')\right| \tag{2.10}$$

Hence, the tidal potential displays spring tides at new and full moon when $\Phi_L=1$, and neap tides at half moon when $\Phi_L=0$. The interval between springs and neaps is about 7.38 days (Doodson & Warburg, 1941).

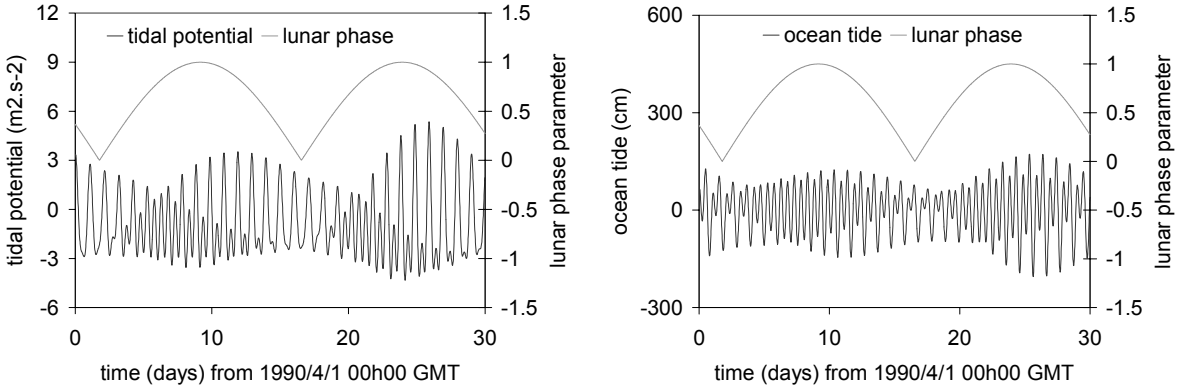

Figure 2.5: 'Amplitude Modulation' of the tidal potential and ocean tide due to changes in the lunar phase parameter (Φ_L) defined in the text, and in Figure 2.4. (a) The tidal potential, W, at the TAG hydrothermal site (26.13°N, 44.82°W). Time-series generated by the ETGTAB code. (b) The ocean tide at the TAG hydrothermal site, generated by the CSR code.

It is important to stress that spring tides *in the oceans* may not occur at the same time as spring tides in the tidal potential. This effect is due to the finite hydrodynamic response time of the oceans. The time lag between Φ_L=1 and oceanic spring tides is known as the age of the tide and varies with location. For example, the tides in British coastal waters generally have an age of about 1.5 days (Manual of Tidal Prediction, 1958). An example of the amplitude modulation caused by lunar phases is presented in Figure 2.5. Unless otherwise stated, the estimates of ocean tide presented in this dissertation have been made using the CSR code, which is derived from satellite altimetry (Schrama & Ray, 1994).

It is reasonable to assume that any tidal signals will display a springs/neaps cycle to some extent. Therefore, when analysing tidal behaviour in a dataset it is important to identify evidence of amplitude modulation, and to correlate this with the springs/neaps cycle in the local ocean tide and tidal potential.

2.3.4 Decomposition into harmonic series

In Sections 2.3.1 – 2.3.3, the tidal potential is viewed as a *non-stationary* mixture of diurnal and semi-diurnal oscillations. This non-stationarity is manifest as amplitude- and frequency modulation of the basic diurnal and semi-diurnal frequencies. However, when viewed over a much longer timescale (~1 year or more) tidal signals can be regarded as *stationary*

harmonic series. In this alternative viewpoint, a tidal signal is decomposed into cosine waves of constant amplitude and frequency.

The relationship between the two viewpoints is exemplified by the following identity (Doodson & Warburg, 1941):

$$f(t) = \underbrace{\left(A + B\cos(\Omega t)\right)}_{L(t)} \cdot \underbrace{\cos(\omega t)}_{S(t)} = \underbrace{A\cos(\omega t)}_{f1(t)} + \underbrace{\tfrac{1}{2}B\cos((\omega+\Omega)t)}_{f2(t)} + \underbrace{\tfrac{1}{2}B\cos((\omega-\Omega)t)}_{f3(t)} \qquad (2.11)$$

Equation (2.11) illustrates how the function $f(t)$, defined by the product $L(t)S(t)$, can be decomposed into the sum $f1(t)+f2(t)+f3(t)$.

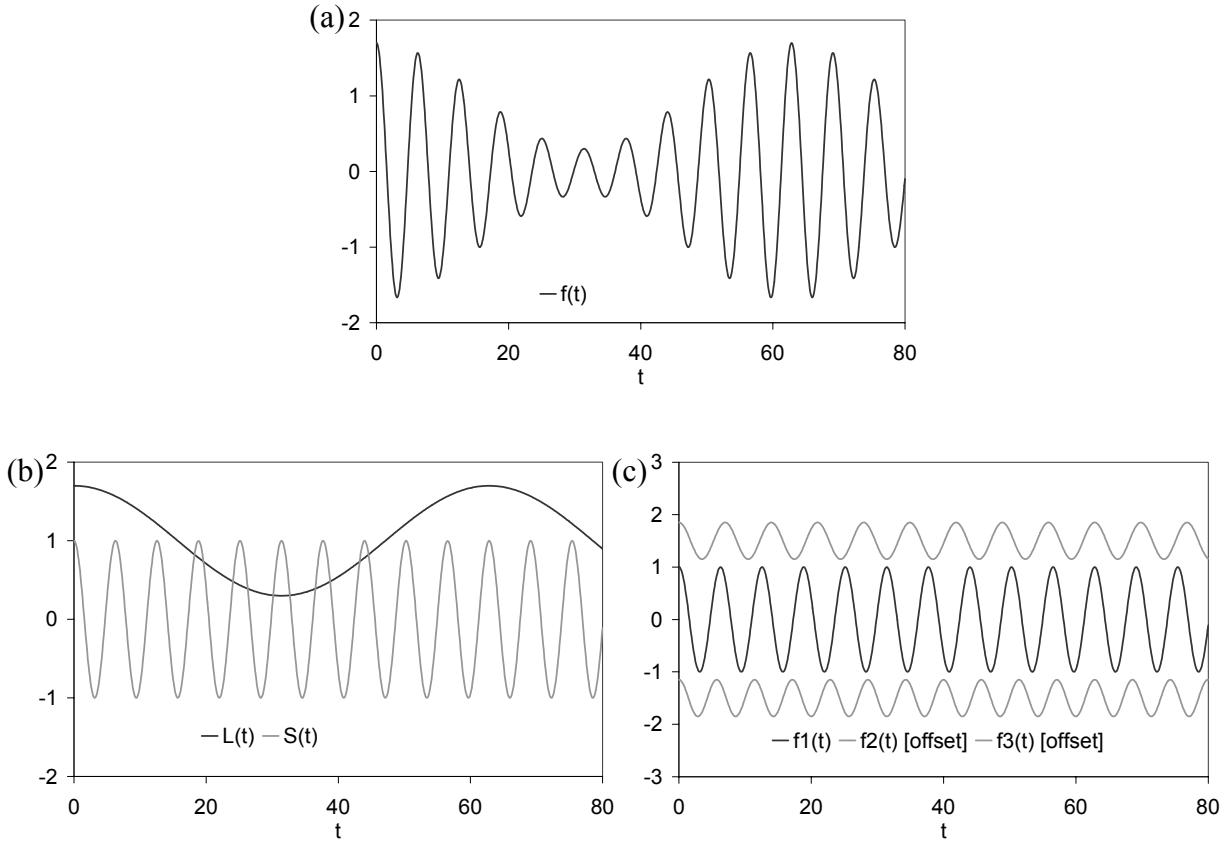

Figure 2.6: The interaction of periodic processes on long and short timescales, illustrated by equation (2.11). (a) The function $f(t)$, which can be decomposed in two ways. (b) Decomposition into a product: $f(t)=L(t)\cdot S(t)$. (c) Decomposition into a sum: $f(t)=f1(t)+f2(t)+f3(t)$. (For clarity, $f2(t)$ and $f3(t)$ have been offset on the y-axis.)

Suppose that $\Omega << \omega$, and that $0<B<A$. The function $f(t)$ is then, in effect, a short timescale process, $S(t)$, (e.g. the daily rotation of the earth), which amplitude-modulated by a long timescale process ($L(t)$) (e.g. monthly changes in lunar declination). Thus, when viewed over a timescale greater than $\sim 1/\Omega$, $f(t)$ is naturally interpreted as an oscillation of angular frequency ω, whose amplitude is not constant, but varies with angular frequency Ω (Figures 2.6a,b). This viewpoint corresponds to the non-stationary species decomposition of Section 2.3.1.

By contrast, the decomposition $f1(t)+f2(t)+f3(t)$ expresses $f(t)$ as a sum of three harmonic terms, each of constant frequency and amplitude (Figure 2.6c).

Thus, the modulation of a short timescale signal of angular frequency ω by a long timescale signal of angular frequency Ω produces a harmonic series of terms with frequencies ω, $(\omega+\Omega)$, and $(\omega-\Omega)$.

This principle lies behind the decomposition of the tidal potential into harmonic components. The (well-known) long-period frequencies of lunar and solar motion combine with the diurnal and semi-diurnal Earth-rotation frequencies to produce a set of N tidal frequencies $\{\omega_1,...,\omega_N\}$. The number of frequencies in a particular decomposition (N) depends on the number of tide-raising bodies included, and the accuracy with which their motions are considered. For example, Doodson (1921) has N=378, Cartwright & Edden (1973) have N=505, and Tamura (1987) has N=1200. A typical tidal spectrum is shown in Figure 2.7.

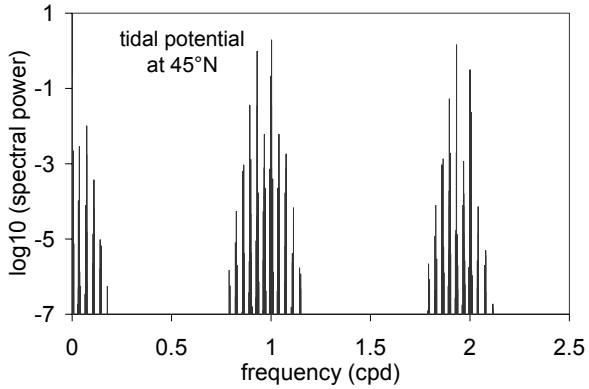

Figure 2.7: A typical tidal power spectrum, calculated from the harmonic constants used in the creation of the time-series in Figure 2.3. The power H_j^2 in each harmonic line is plotted as a function of frequency $\omega_j/2\pi$. Note the logarithmic scale on the y-axis. Data produced using ETGTAB.

After harmonic decomposition, the tidal potential W_2 (at some fixed point on the Earth's surface) is written as a cosine series:

$$W_2(t) = \sum_{j=1}^{N} H_j \cos(\omega_j t - g_j) \tag{2.12}$$

Given a set of tidal frequencies $\{\omega_1,...,\omega_N\}$, the information in the tidal signal $W_2(t)$ is completely described by the set of N amplitudes $\{H_1,...,H_N\}$ and the set of N phase-lags $\{g_1,...,g_N\}$.

The same information can be expressed in complex number notation as follows:

$$W_2(t) = \mathrm{Re}\left(\sum_{j=1}^{N} A_j \exp(i\omega_j t) \right) \tag{2.13}$$

Here, the signal is completely described by the set of N complex numbers $\{A_1,...,A_N\}$.

The amplitude/phase notation and the real/imaginary notation are linked according to:

$$\begin{cases} \mathrm{Re}(A_j) = H_j \cos(g_j) \\ \mathrm{Im}(A_j) = -H_j \sin(g_j) \end{cases} \tag{2.14}$$

The frequency spectrum of $W_2(t)$ is obtained by graphing the power ($H_j^2=|A_j|^2$) in each spectral line against its frequency ($\omega_j/2\pi$). The spectrum in Figure 2.7 is typical and displays the features common to most tidal signals. The spectral lines are clustered into three bands corresponding to the three species of Section 2.3.1 – long-period, diurnal and semi-diurnal. Within each band, certain frequencies tend to contain a greater proportion of the power, and have been assigned names (Doodson & Warburg, 1941). Table 2.1 lists the principal tidal frequencies, along with their names (Doodson & Warburg, 1941).

In the diurnal band, the most significant spectral lines of the tidal potential are *K1*, *O1*, *P1* and *Q1*; and in the semi-diurnal band, they are *M2*, *S2*, *N2* and *K2* (Schwiderski, 1980). The *M2*, or 'principal lunar' component, with a period of 12.42 hours, is usually the most significant component of a tidal signal. For this reason, initial testing of a dataset should involve identification of significant power at ~1.932 cpd which is characteristic of all tidal signals.

Among the harmonic components of the long-period band is a fortnightly component, *Mf*. It is very important to distinguish conceptually between this fortnightly *harmonic component* and fortnightly *modulations*. For example, the springs/neaps cycle is a prominent tidal phenomenon with a period of ~14 days. However, it is caused by the beating of the *M2* and

S2 components, and *not* by the *Mf* component which has an amplitude typically less than 5% of the *M2* component (Schwiderski, 1980).

Consequently, when looking for long-period phenomena in hydrothermal datasets it is more practical to identify long-period modulations than the long-period harmonic components themselves.

name	f (cpd)	T (days)	T (hrs)	name	f (cpd)	T (days)	T (hrs)
M0S0	0.0000	-	-	*J1*	1.0390	0.9624	23.0985
Sa	0.0027	365.2301	8765.5223	*SO1*	1.0705	0.9342	22.4202
Ssa	0.0055	182.6150	4382.7611	*OO1*	1.0759	0.9294	22.3061
STA	0.0082	121.7532	2922.0779	*V1*	1.1122	0.8991	21.5782
MSm	0.0314	31.8120	763.4883	*3N2*	1.8234	0.5484	13.1622
Mm	0.0363	27.5548	661.3149	*ε2*	1.8283	0.5470	13.1273
MSf	0.0677	14.7652	354.3656	*2N2*	1.8597	0.5377	12.9054
Mf	0.0732	13.6608	327.8599	*μ2*	1.8645	0.5363	12.8718
MSTm	0.1046	9.5569	229.3651	*N2*	1.8960	0.5274	12.6583
MTm	0.1095	9.1329	219.1901	*ν2*	1.9008	0.5261	12.6260
MSQm	0.1409	7.0958	170.2989	*γ2*	1.9274	0.5188	12.4519
2Q1	0.8570	1.1669	28.0062	*α2*	1.9295	0.5183	12.4382
σ1	0.8618	1.1603	27.8484	*M2*	1.9323	0.5175	12.4206
Q1	0.8932	1.1195	26.8684	*β2*	1.9350	0.5168	12.4030
ρ1	0.8981	1.1135	26.7231	*δ2*	1.9377	0.5161	12.3855
O1	0.9295	1.0758	25.8193	*λ2*	1.9637	0.5092	12.2218
τ1	0.9350	1.0695	25.6681	*L2*	1.9686	0.5080	12.1916
M1	0.9664	1.0347	24.8333	*2T2*	1.9945	0.5014	12.0329
χ1	0.9713	1.0295	24.7091	*T2*	1.9973	0.5007	12.0165
π1	0.9945	1.0055	24.1321	*S2*	2.0000	0.5000	12.0000
P1	0.9973	1.0027	24.0659	*R2*	2.0027	0.4993	11.9836
S1	1.0000	1.0000	24.0000	*K2*	2.0055	0.4986	11.9672
K1	1.0027	0.9973	23.9345	*ξ2*	2.0369	0.4909	11.7825
ψ1	1.0055	0.9946	23.8693	*η2*	2.0418	0.4898	11.7545
φ1	1.0082	0.9919	23.8045	*M3*	2.8984	0.3450	8.2804
θ1	1.0342	0.9670	23.2070	*M4*	3.8645	0.2588	6.2103

Table 2.1: The principal harmonic components of the tidal potential, derived from the ETGTAB code, listed in order of increasing frequency (*f*). The corresponding period ($T=1/f$) is also shown.

This concept can cause much confusion. For example, Rinehart (1972a, 1972b) attempted to correlate geyser activity with 'the 18.6-year tidal component'. In reality, his study compared geyser activity with the slowly changing amplitude envelope of the tidal oscillations.

It should be stressed that the fixed set of tidal angular frequencies in a particular harmonic decomposition ($\{\omega_1,...,\omega_N\}$) is derived directly from tidal potential – the particular, accurately known signal which gives rise to all tidal phenomena. The harmonic decomposition of *other* tidal signals depends on the assumption that they contain power at precisely the same set of frequencies. Under this assumption, the arbitrary tidal signal $\zeta(t)$ would be written:

$$\zeta(t) = \sum_{j=1}^{N} H_j \cos(\omega_j t - g_j) \tag{2.15}$$

Thus, all of the information in the signal is expressed by the set of N amplitudes $\{H_1,...,H_N\}$ and the set of N phase-lags $\{g_1,...,g_N\}$, collectively known as the harmonic constants of the signal. Unfortunately, for real data, it is rarely possible to determine accurate estimates for all of these harmonic constants. Even if the dataset is free from errors and noise, its finite length will limit the ability to discriminate between individual spectral lines. From Fourier transform theory, it is only possible to separate harmonic components at angular frequencies ω_1 and ω_2 in a time-series whose length exceeds $2\pi/(\omega_1-\omega_2)$ (Press *et al.*, 1986). For example, to separate the *M2* component (period 12.42 hours) from the *S2* component (period 12 hours) requires a time-series of at least 14.8 days duration. The longer the time interval spanned by the dataset the more spectral lines can be extracted. However, to resolve *all* of the spectral lines in a standard harmonic decomposition requires an impractically long time-series of 18.6 years duration, which is the period of revolution of the moon's nodes (Doodson & Warburg, 1941).

The impossibility of resolving all spectral lines from a time-limited dataset renders the classical harmonic decomposition inappropriate for the short, noisy datasets obtained from hydrothermal systems. Consequently, it is important to develop methods of extracting the maximum amount of tidal information from limited datasets. This process is discussed in Chapter 3.

2.4 The Solid Tide

2.4.1 Definition of the Solid Tide

One immediate consequence of the tidal potential is the solid tide, sometimes known as the earth tide. This is defined as the flexing of the solid earth due to the direct influence of the tide-generating force. Of course, the presence of oceans creates an additional tidal strain, due to the changing pressure field which the oceans exert on the seafloor. However, the term tidal loading is reserved for the latter mechanism and it is considered separately, in Section 2.5.4.

2.4.2 The nature of the Solid Tide

It can be shown (Bredehoeft, 1967; Melchior, 1983) that the vertical displacement of the Earth's surface due to the solid tide is:

$$\zeta_s = \frac{h}{g} W_2 \big|_{r=r_E} \tag{2.16}$$

Here, h is a 'Love number' derived from the elastic properties of the Earth and g is gravitational acceleration.

Furthermore, the volumetric dilatation of the crust at the Earth's surface, due to the solid tide, is given by:

$$\varepsilon = \left(\frac{1-2\nu}{1-\nu} \right) \frac{(2h-6l)}{g r_E} W_2 \big|_{r=r_E} \tag{2.17}$$

where ν is a Poisson's ratio, r_E is the radius of the Earth, g is gravitational acceleration and h and l are Love numbers.

The values quoted by Bredehoeft (1967): ν=0.25, h=0.60 and l=0.07, give:

$$\varepsilon \approx \frac{1}{2 g r_E} W_2 \big|_{r=r_E} \tag{2.18}$$

This allows two important conclusions to be drawn. Firstly, the displacements and strains of the solid tide are exactly proportional to, and in phase with, the tidal potential. Secondly, an estimate can be made of the magnitude of the crustal strains due to the solid tide. Oscillations in the tidal potential, W_2, have magnitude ~3 m^2s^{-2} (Figure 2.3). Using $g \sim 9.8$ ms^{-2} and $r_E \sim 6.4 \cdot 10^6$ m suggests that the strain, ε, should have magnitude ~$2.4 \cdot 10^{-8}$. Therefore, the solid tide can be expected to produce strain values of the order of a few tens of nanostrain. Although very small, these strain values are sufficient to cause measurable fluctuation of the water level in wells (Bredehoeft, 1967; Marine, 1975, Rojstaczer & Agnew, 1989).

Furthermore, there is some evidence that the solid tide may influence the periodicity of geysers (Ingebritsen & Rojstaczer, 1993; Ingebritsen & Rojstaczer, 1996). It would therefore seem plausible - *a priori* - that crustal strains created by the solid tide might have an important effect on seafloor hydrothermal systems.

It is important to note that this theory considers the response of the whole Earth to the tide-generating force (Bredehoeft, 1967). The theory does account for changes in the elastic properties of the Earth with depth, but it does not allow for any localised inhomogeneities which might complicate the local strain response.

It is possible to predict the solid tide for any point on the Earth's surface, given values for the Love numbers and Poisson's ratio, since it is proportional to the tidal potential. There are several publicly available codes which perform this calculation, including ETGTAB (H.-G. Wenzel, *pers. comm.*, 1997), and the SPOTL suite of programs (Agnew, 1997)

2.5 The Ocean Tide

2.5.1 Definition of the Ocean Tide

The ocean tide at any particular place ($\zeta_O(t)$) can be defined as the vertical deviation of the sea-surface from its average position due to tidal effects.

2.5.2 The Equilibrium Tide

The equilibrium tide is the ocean tide which would occur on Earth, if two highly idealised conditions were met (Doodson & Warburg, 1941). These conditions are:

(1) There is a single ocean, of constant mean depth, covering the entire globe.

(2) The surface of this ocean achieves instant equilibrium with the tide-raising force. In other words, it is assumed that the ocean surface is always a potential surface, positioned perpendicular to the local effective gravity.

Each of these assumptions represents a considerable departure from the truth, and therefore the equilibrium tide is very different to the true ocean tide in both amplitude and phase.

It can be shown (Doodson & Warburg, 1941) that the equilibrium tide ($\zeta_{eq}(t)$) is simply another scaled version of the tidal potential:

$$\zeta_{eq} = \frac{1}{g} W_2 \big|_{r=r_E} \tag{2.19}$$

The equilibrium tide is very simple to compute, and in the past it has been used as an estimate of the real ocean tide (Thomson *et al.*, 1986). However, there is now such good

knowledge of the true ocean tide (Section 2.5.3), that there is no longer any need to resort to the equilibrium tide.

2.5.3 The Ocean Tide

The real ocean tide observed on Earth is considerably more complex than the equilibrium tide (Schwiderski, 1980). There are many factors which contribute to this complexity, including the topography of the seafloor, the dynamical response of the oceans, friction, Coriolis forces and the presence of coastal boundaries. Nonetheless, the global ocean tide is now known to considerable accuracy. Direct hydrodynamic modelling of the oceans (Le Prevost *et al.*, 1994) and data from satellite altimetry (Schrama & Ray, 1994; Le Prevost *et al.*, 1995) can be combined with data from deep-sea and coastal tide gauges (Egbert at al., 1994) to produce cotidal maps for the principal tidal harmonic components. The maps reproduced in Figure 2.8 are typical, and present a useful summary of the magnitudes of the main tidal components in the world oceans. (Computer codes to predict the ocean tide at any location are currently available at http://podaac-www.jpl.nasa.gov/toppos/toppos_tides.html.)

It is possible to draw some general conclusions about the nature of the ocean tide at different hydrothermal sites, from an analysis of global ocean tide maps (Figure 2.8). For each component of the ocean tide, Coriolis forces create amphidromic points - where the magnitude of the ocean tide is zero - in the open oceans. Amphidromic points are a graphic demonstration of the fact that tides in the middle of the ocean can be very different from those at the coast.

For example, hydrothermal sites on the Mid-Atlantic Ridge, Atlantic Ocean, such as TAG (26.1°N, 44.8°W) and Lucky Strike (37.3°N, 32.3°W), are situated close to the North Atlantic amphidromes and experience much smaller ocean tides than ports on the Atlantic coasts of Europe. In contrast, on the Juan de Fuca Ridge, Pacific Ocean, the Endeavour hydrothermal field (47.8°N, 129.0°W) is situated close to the coast where the ocean tides are reasonably large. There is also a general difference in the spectral nature of the ocean tide in the Atlantic and Pacific Oceans. The natural frequency of oscillation of the Atlantic Ocean is close to two cycles per day. Consequently, the components of the ocean tide in the semi-diurnal frequency band are amplified (Doodson & Warburg, 1941; Figure 2.8). Therefore, the ocean tides of the Atlantic are generally semi-diurnal.

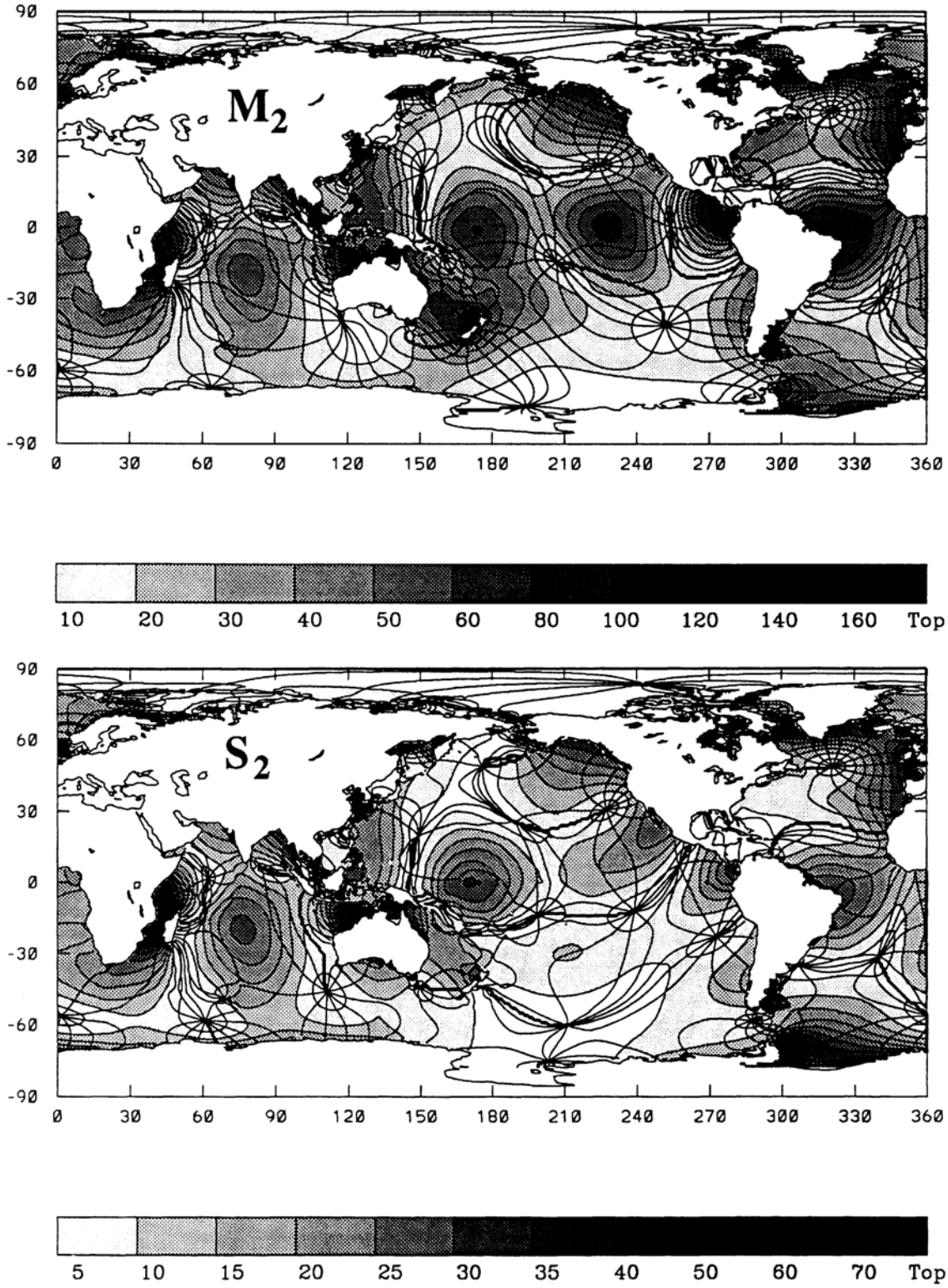

Figure 2.8: (a) Cotidal maps for the semi-diurnal components *M2* and *S2*. Amplitudes are in cm. Cophase lines are drawn at intervals of 30° with the thick line corresponding to the Greenwich passage of the tidal potential. (From Le Prevost *et al.*, 1994).

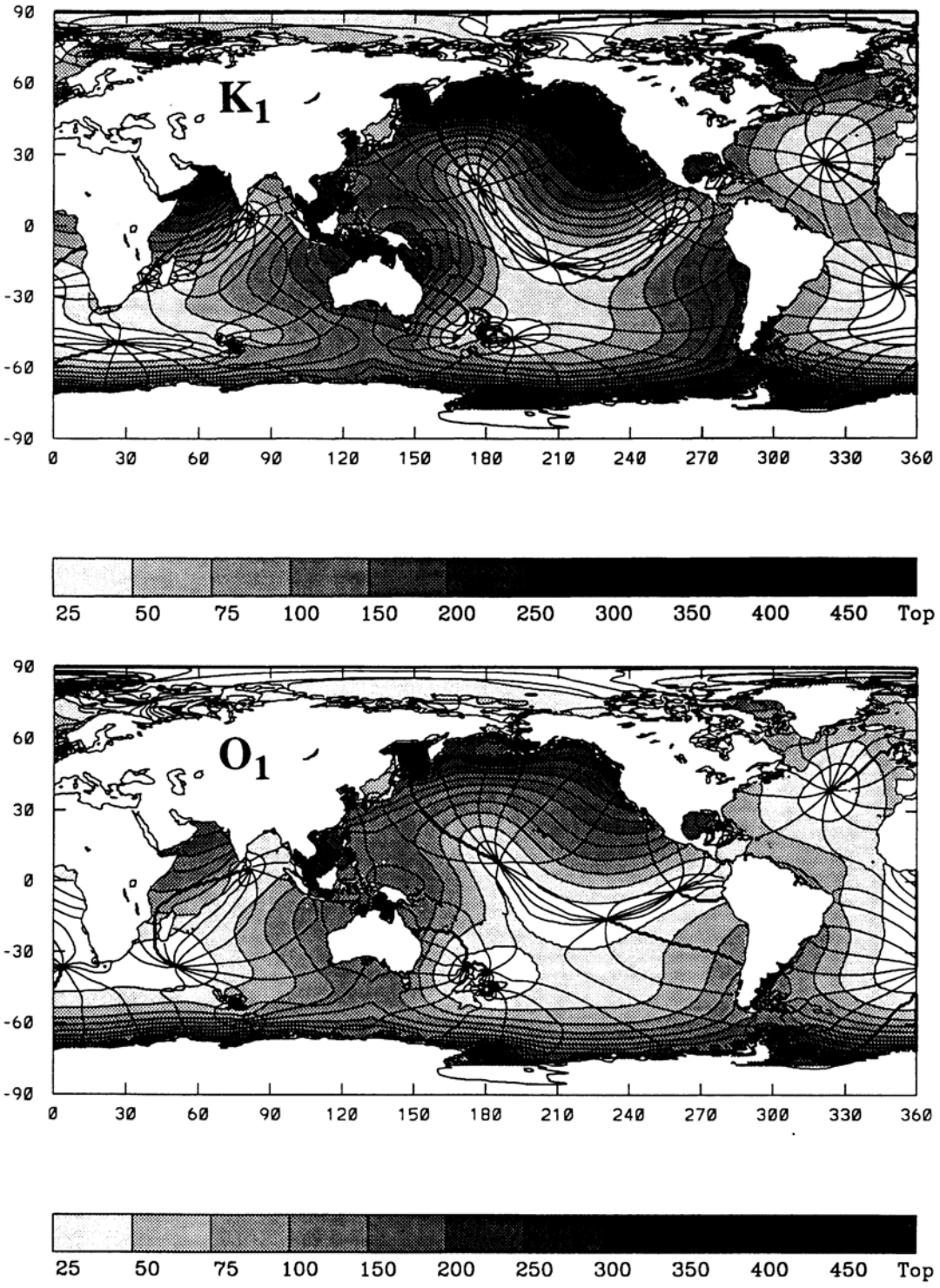

Figure 2.8: (b) Cotidal maps for the diurnal components *K1* and *O1*. Note that amplitudes are in mm, unlike those in Figure 2.8a. Cophase lines are drawn at intervals of 30º with the thick line corresponding to the Greenwich passage of the tidal potential. (From Le Prevost *et al.*, 1994).

Although the frequency modulation of Section 2.3.2 does occur, the small amplitude of the diurnal components renders it insignificant in many cases. In contrast, the Pacific Ocean does not display any particular semi-diurnal resonance. As a result, the diurnal components of the ocean tide are generally much larger in the Pacific Ocean than the Atlantic Ocean (Figure 2.8).

Ideally, direct measurements of the ocean tide could be made, using seafloor pressure sensors, whenever time-series data are acquired from hydrothermal sites. Such sensors would record all changes in seafloor pressure including those which are not tidal in origin, such as the effects of atmospheric pressure and wind. However, where direct measurements are not available, computer simulations of the ocean tide provide a reasonable alternative.

The ocean tides in the open ocean generally have an amplitude of ~1 m, and can be expected to influence hydrothermal systems by imposing a changing pressure field on the seafloor (Section 2.5.4) and by creating horizontal water motion across the seafloor (Section 2.6).

2.5.4 The Load Tide

The ocean tide ($\zeta_O(t)$) (Section 2.5.3), creates a changing pressure field ($\rho_0 g\zeta_O(t)$) on the seafloor, where ρ_0 is the average density of seawater. This generates additional strain and displacement in the Earth's crust - known as the load tide - in addition to the solid tide of Section 2.4. The load tide at any point on the Earth's surface is calculated by evaluating a convolution integral of the ocean tide with the appropriate Green's function over the entire global seafloor (Longman, 1962, 1963; Farrell, 1972a, 1972b, 1973). Thus, the load tide at any point depends on the ocean tide for the whole globe. However, mid-ocean ridge hydrothermal systems are located on the seafloor where the convolution is overwhelmingly dominated by the local ocean tide (Francis & Mazzega, 1990). Therefore, it is an acceptable approximation to assume that load tides on the seafloor are in phase with, and proportional to, the local ocean tide.

For a seawater density $\rho_0 \sim 10^3$ kg.m^{-3}, ocean tides of amplitude ~1 m will create an oscillating seafloor pressure field of amplitude ~10^4 Pa. Ingebritsen & Rojstaczer (1996) considered the crustal strain values expected in land-based hydrothermal systems. They compared the strain magnitude generated by the solid tide with that created by fluctuations in atmospheric pressure. Their argument can be adapted to the investigation of seafloor systems by considering the changing weight of the water column - rather than atmospheric pressure - as the source of the surface load to the crust. Ingebritsen & Rojstaczer (1996) assumed a typical rock compressibility of ~10^{-10} Pa^{-1}, which would suggest that an ocean tide of ~1 m should produce crustal strains of magnitude ~10^{-6}. This is two orders of magnitude greater

than the strains of magnitude ~10^{-8} which are expected to result from the solid tide (Section 2.4). Consequently, it is to be expected that seafloor hydrothermal systems will suffer much more deformation from the load tide (which is proportional to the ocean tide) than from the solid tide (which is proportional to the tidal potential). This expectation is tested in Chapter 4 by comparing hydrothermal time-series with both the local tidal potential and the local ocean tide.

2.6 Tidal Streams

The vertical motion of the sea-surface, defined as the ocean tide ($\zeta_O(t)$), is accompanied by horizontal movement of water within the oceans, which is termed tidal streams (Doodson & Warburg, 1941). Ideally, current meter data would be collected at hydrothermal vent sites concurrently with measurements of temperature, flow rate, pressure and chemistry, but this has not always been possible. In the absence of direct current measurements it is necessary to estimate the tidal streams at hydrothermal vent sites using knowledge (or an estimate) of the ocean tide.

For simplicity, the following sections will consider the tidal stream due to a single tidal component (e.g. the *M2* component), of angular frequency ω. The aim is to summarise the inferences that can be made about tidal streams on the seafloor, given an estimate of the local ocean tide.

2.6.1 Rectilinear travelling waves in the open oceans

In the open oceans the sea-surface displacement due to a particular tidal component takes the form of a travelling wave, progressing rotationally about an amphidrome as illustrated on global co-tidal charts (Figure 2.8). However, for the purposes of this discussion it is sufficient to consider a surface wave in two dimensions (Figure 2.9).

If the wave travels along the x-axis with amplitude A, the displacement of the water surface $\zeta(x,t)$ is given by:

$$\zeta = A\cos(kx - \omega t) \tag{2.20}$$

The dispersion relation is (Lamb, 1932):

$$\omega^2 = gk\tanh(kh) \tag{2.21}$$

and the horizontal and vertical components of the water velocity are:

$$u = A\omega \frac{\cosh(kz + kh)}{\sinh(kh)} \cos(kx - \omega t) \tag{2.22}$$

$$w = A\omega \frac{\sinh(kz + kh)}{\sinh(kh)} \sin(kx - \omega t) \tag{2.23}$$

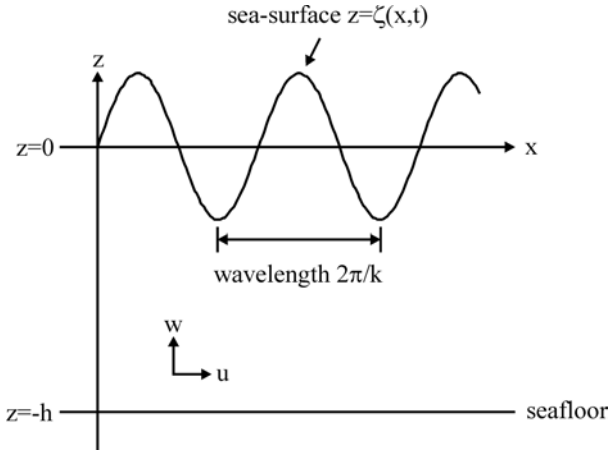

Figure 2.9: The ocean tide ($\zeta(x,t)$) in water of depth h results in a wave of wavenumber k. As described in the text, the nature of the induced tidal stream (u,w) depends on whether this is a standing wave or a travelling wave. The velocity is $u(x,z,t)$ in the x-direction, and $w(x,z,t)$ in the z-direction.

In the open oceans, h is typically ~1 km, while the wavelength $2\pi/k$ is typically ~10^2 – 10^4 km. Hence, kh<<1, and so $\sinh(kh) \approx kh$ and $\tanh(kh) \approx kh$. Under this shallow water approximation, it follows that the horizontal stream, u, on the ocean floor $z = -h$, is an oscillation of magnitude:

$$\frac{A\omega}{\sinh(kh)} \approx A\sqrt{\frac{g}{h}} \tag{2.24}$$

Thus, for a typical ocean tide of amplitude $A \approx 1$ m, in an ocean of depth $h \approx 1000$ m, with $g \approx 10$ m.s^{-2}, the tidal streams would have a magnitude $|u| \sim 0.1$ m.s^{-1}. The surface displacement (ζ) and the horizontal velocity (u) are both dependent on time via the term $\cos(kx-\omega t)$. Therefore peak tidal streams on the ocean floor coincide with low and high tide. This result seems to contradict common experience that slack water occurs at high and low tide, and that peak tidal streams coincide with half-tide. The apparent confusion results because common experience is based on the standing waves found in small gulfs and

estuaries rather than the travelling waves found in the open oceans (Doodson & Warburg, 1941).

2.6.2 Rectilinear standing waves in small gulfs

In a short gulf, for example the Gulf of California (Little *et al.*, 1988), the surface displacement (ζ) due to a particular tidal component often takes the form of a standing wave. The pattern of cophase lines on a cotidal chart (Figure 2.8) reveals whether the surface wave generated by a particular tidal component is a standing wave or a travelling wave. A standing wave of amplitude A can be written as the sum of two travelling waves:

$$\zeta = A\left[\frac{1}{2}\cos(kx-\omega t)+\frac{1}{2}\cos(kx+\omega t)\right] = A\cos(kx)\cos(\omega t) \tag{2.25}$$

By linearity, and using the theory of Section 2.6.1, it follows that the horizontal component of velocity (u) is given by:

$$u = A\omega\frac{\cosh(kz+kh)}{\sinh(kh)}\sin(kx)\sin(\omega t) \tag{2.26}$$

Thus, assuming $kh<<1$, the magnitude of the streams on the seafloor is the same as for travelling waves:

$$\frac{A\omega}{\sinh(kh)} \approx A\sqrt{\frac{g}{h}} \tag{2.27}$$

However, the phase relationship between the ocean tide and tidal streams is very different. The surface displacement (ζ) depends on time via the term $\cos(\omega t)$, but the horizontal velocity (u) depends on time via the term $\sin(\omega t)$. It therefore follows, in agreement with common experience, that peak streams occur at half-tide for standing waves. The interaction of standing and travelling waves in the Gulf of California is discussed in greater detail in Chapter 4.

2.6.3 The frequency spectrum of a rectilinear tidal stream

Consider the horizontal velocity (u) of a rectilinear tidal stream along the x-axis, due to a single tidal component of angular frequency ω, so that $u\sim\sin(\omega t)$. The rate of heat transfer from the seafloor to the ocean is proportional to the speed ($|u|$) of the stream. In contrast, the pressure drop due to flow over a hydrothermal edifice, caused by the Bernoulli effect, is proportional to the square of the speed ($|u|^2$) (Schultz & Elderfield, 1997). Both of these processes might be expected to affect hydrothermal systems, and it is useful to consider the expected spectral nature of signals which depend on them. The square of the speed of the tidal stream is:

$$|u|^2 \sim \sin^2(\omega t) = \frac{1}{2} - \frac{1}{2}\cos(2\omega t) \tag{2.28}$$

Hence, any process which depends linearly on the Bernoulli effect will have all power concentrated at angular frequency 2ω, or twice the angular frequency of the surface displacement.

In contrast, the speed of the tidal stream is:

$$|u| \sim |\sin(\omega t)| = \frac{2}{\pi}\left[1 - 2\sum_{n=1}^{\infty}\frac{1}{(2n+1)(2n-1)}\cos(2n\omega t)\right] \tag{2.29}$$

Hence, any physical process which depends linearly on the rate of heat transfer from the seafloor to the ocean will have spectral power at all of the angular frequencies {2ω, 4ω, 6ω,...}.

Thus, careful examination of the power spectrum of a seafloor tidal signal can be used to distinguish $|u|$-dependent processes from $|u|^2$-dependent processes. However, it must be stressed that the situation is considerably more complicated if the effects of more than one tidal component are significant.

2.6.4 Rotating tidal streams

In many cases, the seafloor tidal streams associated with a particular tidal component are rotating rather than rectilinear (Doodson & Warburg, 1941). In such a case, the vector representing the tidal stream in the horizontal plane traces an elliptical path during each tidal period. If the *x*- and *y*-axes are placed along the major- and minor-axes of this ellipse, then the components of the tidal stream velocity are:

$$u = a\cos(\omega t) \tag{2.30}$$

$$v = b\sin(\omega t) \tag{2.31}$$

It then follows that the square of the speed of the tidal stream is given by:

$$u^2 + v^2 = \frac{1}{2}(a^2 + b^2) + \frac{1}{2}(a^2 - b^2)\cos(2\omega t) \tag{2.32}$$

which has all power concentrated at angular frequency 2ω, as for the rectilinear case (equation (2.28)).

In contrast, the speed of the stream is given by:

$$\sqrt{u^2 + v^2} = \sqrt{\frac{1}{2}(a^2 + b^2) + \frac{1}{2}(a^2 - b^2)\cos(2\omega t)} \tag{2.33}$$

The exact Fourier series representation of this expression is not known, but it is clear that it must contain spectral lines at the angular frequencies {2ω, 4ω, 6ω,...} in the same manner as

equation (2.29). Hence, the same general conclusions can be drawn for the case of rotating streams as for rectilinear streams. In principle, $|u|$-dependent processes could be distinguished from $|u|^2$-dependent processes by examining the spectral power at the even harmonics of the fundamental frequency.

2.7 Conclusions

A tidal signal is defined to be the part of a time-series which is caused by the tidal potential. Several first order tidal signals have been described – the solid tide, ocean tide, load tide and tidal streams, and their potential influence on hydrothermal systems has been discussed.

The solid tide is in phase with the tidal potential and easily predictable using public domain computer codes. It is expected to lead to crustal strains of magnitude $\sim 10^{-8}$ (i.e. tens of nanostrain).

The global ocean tide is extremely complex, but a combination of satellite altimetry, hydrodynamic modelling and pressure gauge data means that it is known to considerable accuracy in most of the world's oceans. There are public domain computer codes which predict the ocean tide at any location. Ocean tides generally have an amplitude of ~1 m. The ocean tide creates a changing pressure field on the seafloor which gives rise to crustal strain – the load tide.

To a reasonable approximation, the load tide at a point on the seafloor is in phase with, and proportional to, the local ocean tide. The crustal strains due to the load tide can be as large as 10^{-6}, two orders of magnitude greater than the solid tide. It is therefore expected that the ocean tide will have a greater influence on hydrothermal systems than the solid tide. This expectation is tested in Chapter 4.

The tidal streams which accompany the ocean tide typically have a magnitude ~0.1 $m.s^{-1}$ in the open ocean. If tidal streams influence hydrothermal systems, it might be informative to examine the power spectrum of hydrothermal tidal signals. A spectrum containing the 4^{th} and 6^{th} harmonics of the tidal frequencies would suggest that the hydrothermal system is influenced by the speed of the water (via heat transfer from the seafloor) rather than the speed squared (via the Bernoulli effect).

The nature of the tidal potential has been examined in some detail, as it is expected that tidal signals in hydrothermal systems will display similar behaviour. When considered over a long time interval (perhaps a year or more), it is reasonable to view tidal signals in terms of their stationary harmonic decomposition, or Fourier series. However, the number of spectral lines which can be resolved from a short dataset (of a few days to a few months) is severely limited. Accordingly, when considering tidal phenomena over the course of a few semi-diurnal cycles it is conceptually useful to view the tidal potential as a mix of diurnal and semi-diurnal frequencies which is frequency- and amplitude-modulated by lunar and solar motions.

The tidal potential can be considered to be amplitude-modulated by the phases of the moon, and frequency-modulated by the lunar and solar declinations. It is informative to look for similar behaviour in time-series obtained from hydrothermal systems (Chapter 4). The astronomical positions of the sun and moon are accurately known, and are expected to influence *all* tidal signals in a similar way. Consequently, it is efficient to use this astronomical knowledge to develop data analysis techniques which are specifically designed for use with tidal time-series. Chapter 3 is concerned with the development of these techniques.